Elsevier Editorial System(tm) for Journal of Magnetism and Magnetic Materials
Manuscript Draft

Manuscript Number: MAGMA-D-14-00698

Title: Synthesis and characterization of ZnxFe3-xO4 nanoparticles with tunable magnetic properties

Article Type: Regular Submission

Keywords: magnetic nanoparticles, ferrites

Corresponding Author: Ms. Elena Petrova, MSc

Corresponding Author's Institution: Belarusian State University

First Author: Elena Petrova, MSc

Order of Authors: Elena Petrova, MSc; Dzmitry Kotsikau, Ph.D.; Vladimir Pankov, Ph.D., Prof.

Abstract: Nanocrystalline ZnxFe3-xO4 solid solutions (with x = 0, 0.18, 0.45, 1) with crystallite sizes of 5-10 nm, specific surface of about 180 m2/g and narrow size distribution were synthesized via an inorganic variant of sol-gel approach. The composition and structure of the formed nanoparticles were characterized by XRD, SEM, TEM, ICP-AES and FTIR spectroscopy. Hysteresis loops recorded for the samples indicate their ferromagnetic behavior at 5 K and superparamagnetic behavior at 300 K. The highest maximum magnetization of 59 emu/g at room temperature corresponds to Zn0.18Fe2.82O4 composition, and at 5 K - to Zn0.45Fe2.55O4 (86 emu/g), both exceeding the saturation magnetization of pure magnetite.

*Cover Letter

Cover letter

Elena Petrova
Belarusian State University, Physical Chemistry Department
220030, Belarus, Minsk, Leningradskaya str. 14, r.607

05.05.2014

I am enclosing herewith a manuscript entitled “Synthesis and characterization of $Zn_xFe_{3-x}O_4$ nanoparticles with tunable magnetic properties” for publication in Journal of Magnetism and Magnetic Materials for possible evaluation. The Corresponding author of this manuscript is Elena Petrova MSc, and contribution of the authors as mentioned below with their responsibility in the research.

1. Dzmitry Kotsikau, Ph.D. (Belarusian State University, Physical Chemistry Department)
2. Vladimir Pankov, Ph.D., Professor (Belarusian State University, Physical Chemistry Department, Head of the Department)

We confirm that this work is original and has not been published elsewhere nor is it currently under consideration for publication elsewhere.

In this paper, we report on the synthesis of superparamagnetic Zn-doped magnetite nanoparticles via modified inorganic sol-gel technique. The magnetic properties of these nanomaterials were investigated at low and room temperatures and compared with those of magnetite in the point of view of potential biomedical applications, e.g. as magnetic resonance imaging (MRI) contrast agents. The paper should be of interest to readers in the areas of magnetic iron oxides synthesis, modification and characterization.

Please address all correspondence concerning this manuscript to me at petrovaeg@bsu.by.

Thank you for your consideration of this manuscript.

Sincerely,

Elena Petrova.

Synthesis and characterization of $Zn_xFe_{3-x}O_4$ nanoparticles with tunable magnetic properties

E. Petrova[1], D. Kotsikau[1], V. Pankov[1]
[1]*Belarusian State University, Department of Physical Chemistry, Minsk, Belarus, Leningradskaya str. 14*
e-mails: petrovaeg@bsu.by, kotsikau@bsu.by, pankov@bsu.by

Corresponding author: Elena Petrova (petrovaeg@bsu.by). 220030 Belarus, Minsk, Leningradskaya str. 14, r.607. Phone number: +375 17 209 57 11, +375 29 764 92 52.

Abstract

Nanocrystalline $Zn_xFe_{3-x}O_4$ solid solutions (with x = 0, 0.18, 0.45, 1) with crystallite sizes of 5-10 nm, specific surface of about 180 m^2/g and narrow size distribution were synthesized via an inorganic variant of sol-gel approach. The composition and structure of the formed nanoparticles were characterized by XRD, SEM, TEM, ICP-AES and FTIR spectroscopy. Hysteresis loops recorded for the samples indicate their ferromagnetic behavior at 5 K and superparamagnetic behavior at 300 K. The highest maximum magnetization of 59 emu/g at room temperature corresponds to $Zn_{0.18}Fe_{2.82}O_4$ composition, and at 5 K – to $Zn_{0.45}Fe_{2.55}O_4$ (86 emu/g), both exceeding the saturation magnetization of pure magnetite.

Highlights

- Modified inorganic sol-gel method was developed to produce ZnxFe3-xO4 nanoparticles
- Nanoparticles exhibit narrow size distribution with a particle size of 5-10 nm
- The compositions with a higher magnetization value than magnetite were obtained
- All the $Zn_xFe_{3-x}O_4$ nanoparticles are superparamagnetic at room temperature

KEYWORDS: magnetic nanoparticles, ferrites.

1. Introduction

At present time, nanosized ferrite particles with a spinel-type structure are being widely used in biology, medical diagnostics and therapy. In particular, *in vivo* applications, in therapeutic (hyperthermia and drug-targeting) and diagnostic applications (nuclear magnetic resonance (NMR) imaging), while for *in vitro* applications the main use is in diagnostics (separation/selection and magnetorelaxometry). The preparation of magnetic nanoparticles for the application in biomedicine includes such techniques as precipitation and coprecipitation from solutions, microemulsion synthesis, polyol technique, high-temperature decomposition of organic precursors, spray and laser pyrolysis etc. [1].

Magnetic nanoparticles based on iron oxides, such as magnetite (Fe_3O_4) or maghemite (γ-Fe_2O_3), are the most commonly employed for biomedical applications. Superparamagnetic iron oxide nanoparticles are widely used, for example, as T2 contrast agents for magnetic resonance imaging (MRI) [2-4]. For some applications a high magnetization of the particles is also required so that their migration in blood stream could be controlled with an external magnetic field and they could be immobilized close to the target pathologic tissue [5]. However, it still remains an open challenge to improve the magnetic properties of superparamagnetic iron oxide nanoparticles, which would lead to a higher imaging sensitivity. The vast majority of research work is devoted to the synthesis of pure oxide materials, even though the preparation of mixed oxide compositions may contribute to a considerably broader range of their functional properties. One of the ways to improve the magnetic properties of the nanoparticles is doping of magnetite with zinc with the formation of zinc ferrite – magnetite solid solutions.

The magnetic properties of zinc ferrite reported so far are related to the cation distribution [6]. Zinc ferrites are generally denoted as $(Zn_yFe_{1-y})[Zn_{x-y}Fe_{2-x+y}]O_4$, where the parentheses and

square brackets refer to the cations occupying tetrahedral site (A sites) and octahedral site (B sites), respectively. When an external magnetic field is applied, the magnetic spins of atoms at B sites align in parallel with the direction of the external magnetic field, but those at A sites align antiparallel. Since the number of B sites is twice that of the A sites, a non-compensated magnetic moment occurs due to the dominant A–B interactions. It has been demonstrated that the addition of $ZnFe_2O_4$ ferrite to an inverse spinel structure (e.g., Fe_3O_4) can increase the net magnetic moment of the resulting mixed spinel structure [7].

There is also another advantage of Zn-substituted iron oxide nanoparticles in comparison with other ferrites the reduced toxicity of Zn over other metals. A preliminary in vitro cytotoxicity test suggests that the zinc ferrite nanoparticles possess a good safety profile [8]. For example, the Food and Drug Administration has set the reference daily intake doses for Zn at 15 mg/day, respectively, which is much higher than the Mn value (2 mg/day) [9].

A variety of methods of preparation of zinc ferrite nanoparticles has been proposed. Among them are mechanical milling [10], co-precipitation method [11], rapid quenching method [12], pulsed laser deposition technique [13], sol gel route [14], approach based on oil-in-water micelles [7], sputtering method [15], solvothermal processing [16]. The reported data show that the physical and chemical properties of the nanomaterials are strongly dependent on the used synthetic route.

As it was shown earlier, a modification of sol-gel method based on inorganic precursors is a promising approach to obtain advanced metal oxide materials for different applications [17-19]. The sol-gel approach provides major possibilities to modify grain size, nanostructure and phase composition of metal oxide materials, and, consequently, to tailor their functional properties in a wide range. This is achieved by varying the nature and concentration of precursors, precipitants and stabilizing agents; the temperature of the reaction mixture; the order and the rate of reagents mixing; pH level of solutions; the mode of heat treatment of the product. The variations of the sol-gel method allow nanomaterials to be prepared in forms of sol, powder, film and ceramics. These techniques are based on the precipitation of metal hydroxides and consecutive transformation of the precipitate into sol, gel, xerogel and crystalline oxide [19].

For most biomedical applications, it is strictly important to obtain single-phase products homogeneous in the composition and structure. A co-precipitation of metal hydroxides and subsequent transformation of the sediment into sol state provide a high degree of homogeneity of the starting components in reactant solutions thus promoting an efficient interaction between them. As a result, multicomponent oxide materials with a highly homogeneous structure are obtained, which cannot be achieved by using the conventional ceramic approach [20]. In the presence of bivalent metals like Fe^{2+} and Zn^{2+}, the preparation of homogeneous and stable colloidal solutions becomes a more complicated task. Therefore, a grounded selection of optimal reaction conditions are required.

In this study, we successfully synthesized the nanoparticles of zinc-substituted magnetite with different composition via modified inorganic sol-gel technique. The magnetic properties and crystal structure of the $Zn_xFe_{3-x}O_4$ solid solutions were systematically investigated in the view of their potential biomedical applications.

2. Experimental

2.1. Sample preparation

Nanoparticles of $Zn_xFe_{3-x}O_4$ (with x = 0.18, 0.45, 1) and magnetite, Fe_3O_4, were prepared at room temperature by a modified inorganic sol-gel technique from water solutions of inorganic salts. $Fe(NO_3)_3 \cdot 9H_2O$, $Zn(NO_3)_2 \cdot 6H_2O$ and $FeSO_4 \cdot 7H_2O$ taken in stoichiometric proportion (with 5% excess of $FeSO_4 \cdot 7H_2O$ to compensate a possible oxidation of Fe^{2+} ions to Fe^{3+}) were dissolved in water at room temperature to form a clear solution. To remove oxygen, water was purged with nitrogen for 40 min with a flow rate 25 ml/s. The solutions of all salts were then mixed together under vigorous stirring and left stirred for 30 min. At this stage of the synthesis, a hydrolytic interaction between salts starts due to the pH difference of the solutions of individual

salts. The solution of salts was added under vigorous stirring to a concentrated solution of NaOH, which was taken in 20 % excess. Under the indicated precipitation conditions, an instantaneous formation of small-sized product aggregates is realized, which allows us to obtain a stable colloidal solution of nanosized (less than 10 nm) particles with a narrow size distribution. The suspension was stirred for one hour to ensure the processes of hydrolysis, particle growth, polycondensation of oxo- and hydroxocomplexes and recrystallization were completed. The described reversed order of mixing the reactants together with the excess of the precipitant provides the preservation of phase and chemical homogeneity for each nanoparticle in the growth process since pH of the suspension is maintained constant (~11) throughout the reaction. This pH value is sufficient for complete deprotonation of the aquacomplexes of all three metal ions – Fe^{3+}, Fe^{2+} and Zn^{2+}, but not for the formation of noticeable amount of water-soluble metal hydroxocomplexes. Furthermore, a precipitation of mixed iron-zinc oxohydroxide with a cubic structure similar to the crystal lattice of the target spinel is expected at early stages of the hydrolysis. A consecutive process including the formation of individual hydroxides and their interaction is not typical of the given synthesis conditions [21].

To obtain a pure product of desired chemical composition and to ensure a long-term stability of the corresponding colloidal solution, it is necessary to remove anions of the used salts from the resulting suspension. After washing the precipitate by decantation with water for three times, a peptization occurred spontaneously giving a sol. The sol was stable under centrifugation at 6000 rpm due to the stabilizing effect of the residual hydroxyl ions adsorbed on the oxide aggregate. However, a significant amount of nitrate and sulfate anions remained in the sol thus far. To remove these anions, the pH of the sol was adjusted to ~7 by adding a 1% solution of HNO_3. At this acidity level, an isoelectric point of the oxide surface was reached causing the coagulation of the sol. The precipitate was washed with small portions of water (50 ml) three times under centrifugation, and then peptized by adding a diluted NaOH solution to pH of 8 followed by ultrasonic treatment (3 min, 22 kHz). As a result, a stable transparent brown sol was obtained. To prepare powdered samples, the sol was dried at 60 °C in air.

2.2. Characterization

Phase composition and grain size of the samples were studied by powder X-ray diffraction (XRD). The XRD analysis was carried out using Co-Kα radiation in 2θ range of 10-120°. The lattice constants were refined using RTP 3.3 X-ray structure tabular processor. Average crystallite size (d_{XRD}) was estimated from the broadening of diffraction lines using the Scherrer equation, $d_{XRD} = K\lambda/[(B-b)\cos\theta]$, with the wave length λ, the peak width B, the instrumental broadening b, the Bragg angle θ and the shape factor $K \approx 0.89$.

In addition to the XRD analysis, fine structural features of the ferrites were revealed using infrared spectroscopy method (IR). IR spectra were recorded on an AVATAR FTIR-330 spectrometer supplied with a Smart Diffuse Reflectance accessory in wavenumber (λ) range of 400-4000 cm^{-1}.

Specific surface area (A_s) of the powders was determined by nitrogen adsorption (BET, ASAP 2020). Assuming spherical shape of the particles, their average size (d_{BET}) was estimated using the relation $d_{BET} = 6/\rho A_s$ with the density ρ.

Morphology of the materials was characterized with a LEO 1420 scanning electron microscope (SEM), and a LEO 906E transmission electron microscope (TEM).

Composition of the particles was estimated by inductively coupled plasma atomic emission spectrometry (ICP-AES) with an ACTIVA-M ICP-AES spectrometer.

Magnetization measurements were performed with a Cryogen Free Measurement System (CFMS) Cryogenic Ltd. Hysteresis loops, M(H), were recorded at 5 and 300 K. The magnetization at field of 5 T was taken as a maximum magnetization, M_{max}. The magnetization was also recorded as a function of temperature, M(T), between 5 and 330 K in zero-field-cooled (ZFC) and field-cooled (FC, H=60 Oe) modes, respectively.

3. Results and discussion

The composition of the prepared zinc-iron oxides measured by ICP-AES matches closely the theoretically calculated values. For $ZnFe_2O_4$, the content of zinc was found to be 49.8 mol % and for $Zn_{0.18}Fe_{2.82}O_4$ – 11.6 mol %, while the theoretical values are 50.0 and 11.3 mol %, respectively (Table 1). The concentrations of silica and calcium oxide were measured to be very low.

Table 1.
Results of chemical analysis (measured with ICP-AES) of zinc-iron oxide powders prepared by co-precipitation technique: concentrations of main constituents and of calcium oxide and silica impurities.

	Main constituents, mol. %				Impurities, wt. %			
	theoretical		experimental		theoretical		experimental	
	ZnO	Fe_2O_3	ZnO	Fe_2O_3	CaO	SiO_2	CaO	SiO_2
$ZnFe_2O_4$	50.0	50.0	49.8	50.2	-	-	<0.006	<0.006
$Zn_{0.18}Fe_{2.82}O_4$	11.3	88.7	11.6	88.4	-	-	<0.006	<0.006

A typical XRD pattern of the synthesized zinc-iron oxides is shown in Fig. 1. For all samples, the only reflections attributed to a cubic spinel structure (Fd3m space group, PDF # No. 227) were observed. The observed diffraction lines are diffuse and broadened, as expected for the nanocrystalline character of the particles. The lattice constant *a* of the Fe_3O_4, $Zn_{0.18}Fe_{2.82}O_4$, $Zn_{0.45}Fe_{2.55}O_4$ and $ZnFe_2O_4$ solid solutions with average particle sizes of 5–6 nm were calculated to be 8.369, 8.391, 8.397 and 8.425 Å, respectively. It is seen that the lattice constant value increases with the increase in zinc content. The lattice constant calculated for the prepared $ZnFe_2O_4$ is slightly smaller as compared to stoichiometric bulk zinc ferrite (*a* = 8.44 Å), indicating that the spinel structure is cation defective and/or that the crystallization of a homogeneous spinel ferrite is not completed yet. The same decrease in lattice constant was also observed for Fe_3O_4 (*a* = 8.38 Å for bulk magnetite). Another possible explanation could be in a partial oxidation of magnetite to maghemite, γ-Fe_2O_3, for which the lattice parameter is smaller (8.34 Å).

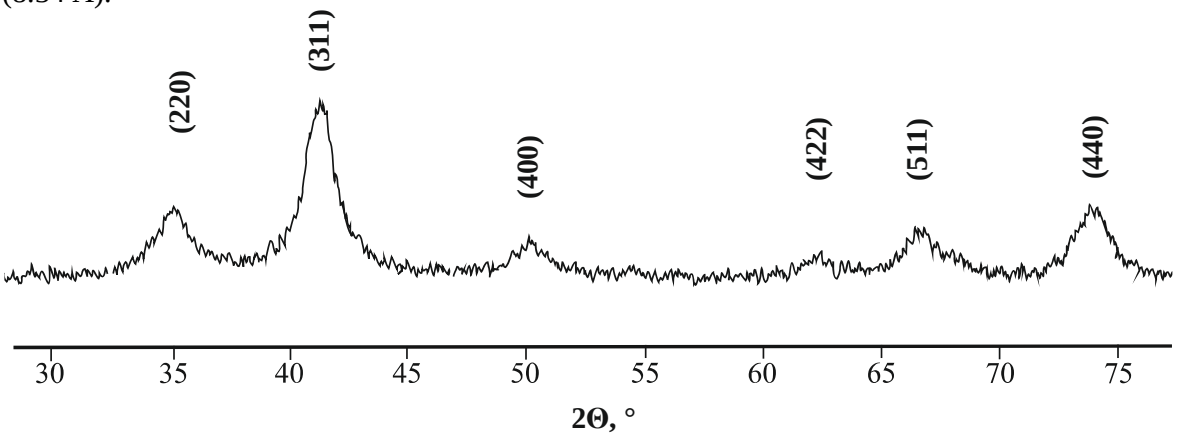

Figure 1. XRD pattern of $Zn_{0.18}Fe_{2.82}O_4$ nanoparticles

All the ferrite samples exhibit a developed specific surface area of 170-180 m^2/g, which corresponds to a particle size of about 6 nm. The diameter estimated from the BET data matches well the average particle sizes calculated by the Scherrer equation.

To clarify the character of zinc distribution in the synthesized ferrites, IR spectroscopy was used. This method also provides additional information about the surface state of oxide materials. IR spectra of the magnetite samples heated at 50 °C with different degree of substitution of Fe^{3+} ions with Zn^{2+} ions are compared together in Fig. 2. The absorption bands in λ region of 400-1200 cm^{-1} are only shown. These bands are attributed to the stretching

vibrations of Me□O ($\nu_{Me□O}$ = 400 ÷ 700 cm$^{□1}$) and bending vibrations of Me□O□H ($\delta_{Me□O□H}$ = 800 ÷ 1200 cm$^{□1}$). The occurrence of OH-groups in the ferrites is explained by poor crystallinity of the structure and incomplete dehydration of hydroxides. In addition to the structurally bound hydroxyl groups, the presence of significant amount of adsorbed water is also typical of the xerogels of metal oxides obtained by the inorganic sol-gel method. The adsorbed water remains in the sol-gel derived samples after their annealing at temperatures up to 600 °C. The adsorbed water was registered in the IR spectra as broad absorption bands of $\nu_{H□O□H}$ at ~ 3410 cm$^{□1}$ (not shown in the figure) and relatively narrow peaks of $\delta_{H□O□H}$ at ~ 1630 cm$^{□1}$.

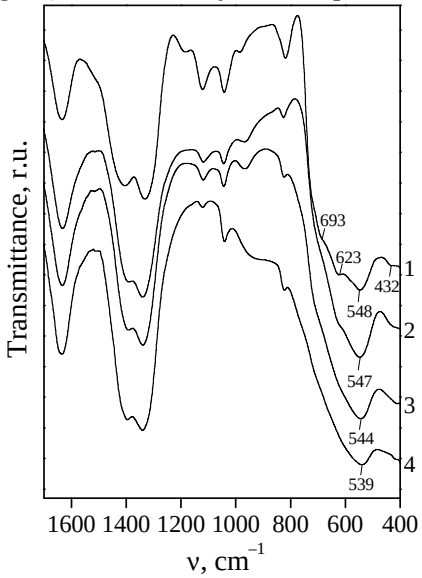

Fig. 2. Fragments of IR spectra of magnetite and zinc-substituted magnetite:
1– Fe_3O_4; 2 – $Zn_{0.18}Fe_{2.82}O_4$; 3 – $Zn_{0.45}Fe_{2.55}O_4$; 4 – $ZnFe_2O_4$

In the IR spectra of all the samples, intense absorption bands of $NO_3^{□}$-groups adsorbed on the oxide surface (1330 and 1400 cm$^{□1}$) were also observed. The presence of nitrate anion is a result of the stabilization of the colloidal solutions with nitric acid.

As it seen from Fig. 2, all the IR spectra differ slightly from each other. The distinctions appear as shifts of the absorption bands to higher frequencies (lower wavenumbers) as well as changes in the intensity when going from individual magnetite to stoichiometric zinc ferrite. This is due to the substitution of Zn^{2+} ions for Fe^{3+} ones. No absorption bands of individual zinc oxide or hydroxide were detected in the IR spectra of the samples. The reported data confirms the formation of substitutional solid solutions in the samples for all zinc concentrations studied.

The IR spectra of the samples were analyzed in more details in the region of 400÷700 cm$^{□1}$, which is characteristic of the crystalline lattice of oxides. The spectrum of individual magnetite matches well the reference pattern for Fe_3O_4. The characteristic absorption band for magnetite is a band at 548 cm$^{□1}$, which is assigned to the Fe□O stretching mode evoked by the interaction of the iron ions in the octahedral sites of the lattice with oxygen ions. The occurrence of low-intensive additional peaks in the considered frequency range (432, 623 and 693 cm$^{□1}$) indicates the formation of an ordered structure of cation vacancies in the octahedral sites of the inverse spinel lattice [22].

As stated earlier, in $Zn_xFe_{3-x}O_4$ and $Co_xFe_{3-x}O_4$ materials obtained by combined decomposition of oxalates of iron and zinc, or oxalates of iron and cobalt, the formation of substitutional solid solutions is possible in a wide range of concentrations [23]. Iron ions occupying tetrahedral sites of the spinel lattice are replaced with Zn^{2+} or Co^{2+} ions that should lead to the shift of the $\nu_{Fe□O}$ vibration bands to higher frequencies due to increase of the effective mass of $Zn^{2+}□O^{2-}$ complexes. This was also observed for our samples with the increase in the degree of iron substitution with zinc in magnetite. Thus, the wavenumbers of the main

absorption band for Fe_3O_4, $Zn_{0.18}Fe_{2.82}O_4$, $Zn_{0.45}Fe_{2.55}O_4$ and $ZnFe_2O_4$ are 548, 547, 544 and 539 cm^{-1}, respectively.

The intensity of the peaks at 432, 623 and 693 cm^{-1} decreases with the increasing zinc content in the ferrites, which relates to a gradual disordering of the cation vacancies. There is also a similar slight shift of the band at 548 cm^{-1} towards lower wavenumbers. The complete disappearance of this band confirms the formation of normal spinel structure in the case of stoichiometric ferrite $ZnFe_2O_4$.

TEM and SEM micrographs of the ferrites given in Fig. 3 confirm the diameter of the grains ranging from 5 to 10 nm and show that the grains have spherical shape with a quite narrow size distribution.

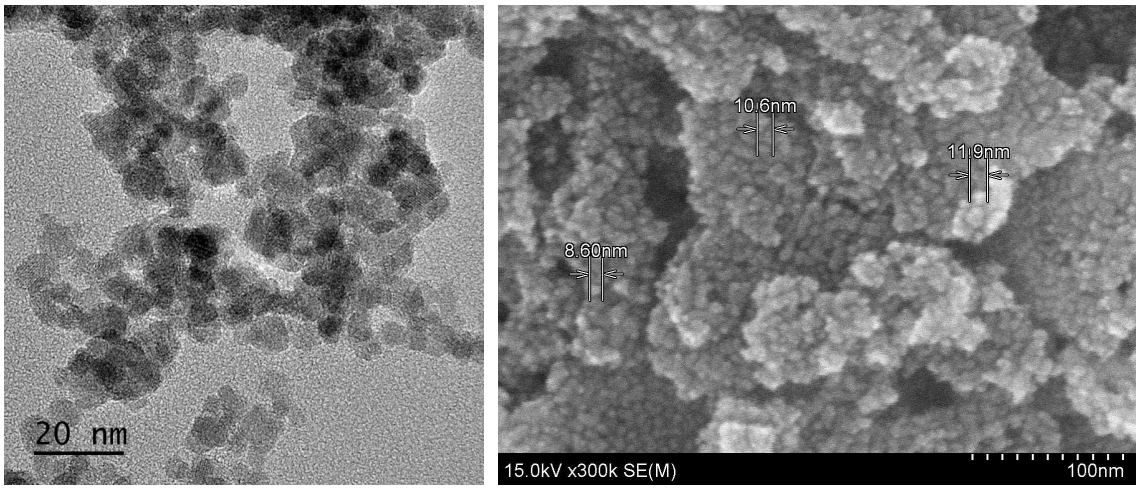

(a) (b)

Fig. 3. TEM (a) and SEM (b) micrographs of $Zn_{0.45}Fe_{2.55}O_4$ nanoparticles

The specific magnetization of the zinc-iron oxide powders as a function of induction of applied magnetic field in is shown Figs. 4 and 5. It is seen that the magnetization of all the solid solutions is not completely saturated at the maximum value of external magnetic field (5 T). At 5 K, all the samples show hysteresis behavior with small, but non-zero coercivities (10-50 Oe for different sample compositions). In contrast, at 300 K, all the samples display no hysteresis. This indicates that in the prepared powders the majority of the particles have a diameter below the size critical for superparamagnetic behavior, which is in agreement with the TEM and XRD data given above.

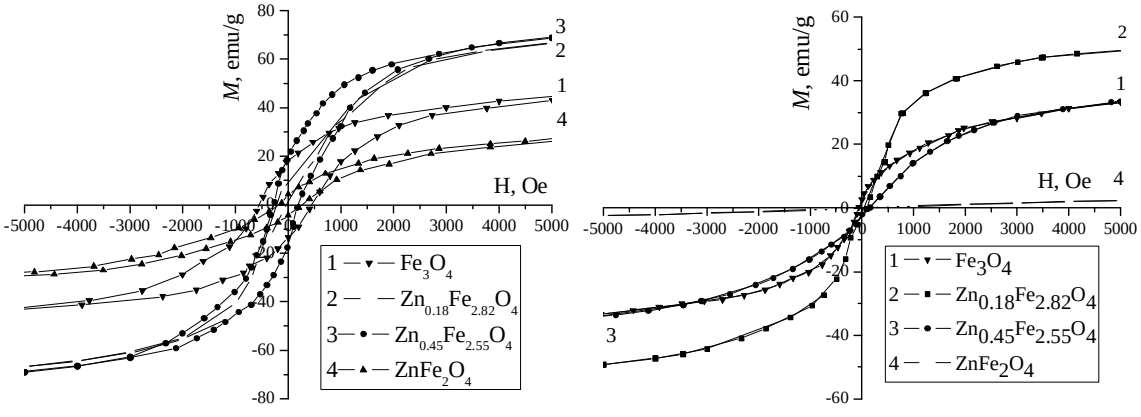

(a) (b)

Fig. 4. Hysteresis loops of $Zn_{0.18}Fe_{2.82}O_4$, $Zn_{0.45}Fe_{2.55}O_4$, $ZnFe_2O_4$ and Fe_3O_4 recorded at 5 K (a) and 300 K (b)

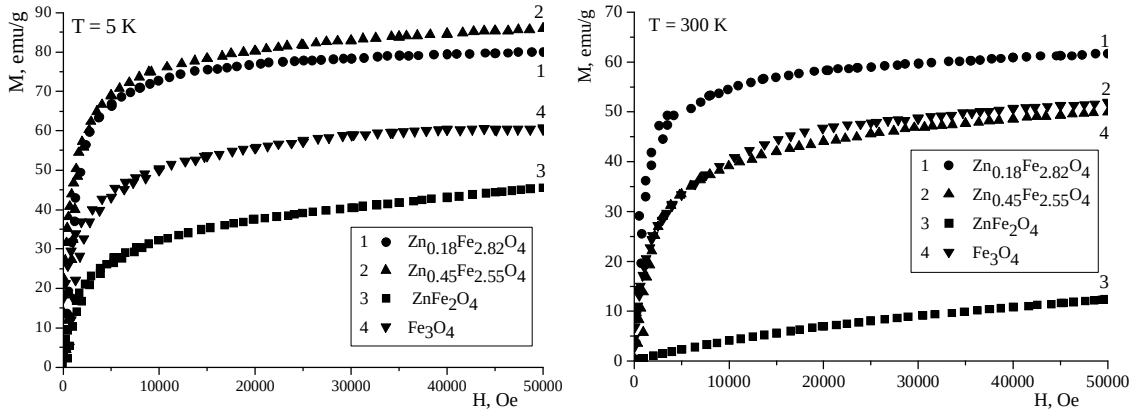

(a) (b)

Fig. 5. Magnetization vs. field for $Zn_{0.18}Fe_{2.82}O_4$, $Zn_{0.45}Fe_{2.55}O_4$, $ZnFe_2O_4$ and Fe_3O_4 recorded at 5 K (a) and 300 K (b)

The maximum magnetization values measured for the Zn-doped samples at 5 and 300 K are compared with pure magnetite in Table 2. The highest maximum magnetization of 86 emu/g measured at 5 K for the $Zn_{0.45}Fe_{2.55}O_4$ sample exceeds noticeably the value for Fe_3O_4 (62 emu/g). This is still lower than the saturation magnetization value of 96 emu/g measured for well crystalline bulk magnetite in [24, 25]. The bulk magnetite structure has an inversed cation distribution and antiparallel alignment of magnetic moments between the A- and B-sites of the spinel lattice. Reduced magnetization values are typical of nanosized ferrites. A possible origin of this phenomenon is in the formation of a surface layer of reduced magnetization, caused by a different composition and cation distribution or disordered spins in the surface of oxides [26, 27].

Table 2.
Maximum magnetization values for $Zn_xFe_{3-x}O_4$ samples and pure magnetite measured at 5 and 300 K (emu/g), blocking temperature T_B and ZFC/FC separation temperature T_S (K)

	$Zn_{0.18}Fe_{2.82}O_4$	$Zn_{0.45}Fe_{2.55}O_4$	$ZnFe_2O_4$	Fe_3O_4
5 K	80	86	45	62
300 K	59	46	9	49
T_B	100	90	25	-
T_S	270	220	36	-

Hysteresis measurements carried out at 300 K have shown superparamagnetic behavior for all the synthesized nanoparticles. The highest maximum magnetization is observed for $Zn_{0.18}Fe_{2.82}O_4$ and is equal to 59 emu/g (for Fe_3O_4 it is 49 emu/g at this temperature), while for $Zn_{0.45}Fe_{2.55}O_4$ M_{max} = 46 emu/g. As it follows from the above results, a maximum of saturation magnetization at a certain Zn content in magnetite is expected. M_{max} of stoichiometric Zn ferrite ($ZnFe_2O_4$) is the lowest at both 5 and 300 K (45 and 9 emu/g, respectively), which is evidently due to a predominant Zn^{2+} occupation of A sites instead of B sites in the spinel lattice leading to a decrease in the magnetic parameters of the material.

Zero field cooled (ZFC) and field cooled (FC) measurements of $Zn_{0.18}Fe_{2.82}O_4$ and $Zn_{0.45}Fe_{2.55}O_4$ samples represented in Figs. 6-a and b show a behavior typical of superparamagnetic particles with a significant width of the particle size distribution. The ZFC curve separates from the FC curve at T_s and goes through a maximum at blocking temperature T_B. The analysis of the ZFC/FC curves can provide some additional information about the cluster state of the sample. The derivative of this curve is correlated with the temperature distribution of the energy barrier, which in turn is connected with a particle size distribution. The separation point position of ZFC/FC curves corresponds to the maximum blocking temperature (and a

maximum particle size), whereas the peak position on ZFC curve corresponds to the average blocking temperature value. The relatively small difference between T_B and T_S (~10 K) and a sharp FC maximum in Fig. 6-c indicate a narrow particle size distribution for $ZnFe_2O_4$, which was not observed for both $Zn_{0.18}Fe_{2.82}O_4$ and $Zn_{0.45}Fe_{2.55}O_4$ compositions. The ZFC curves recorded for $Zn_{0.18}Fe_{2.82}O_4$, $Zn_{0.45}Fe_{2.55}O_4$ and $ZnFe_2O_4$ display a hill at 100, 90 and 25 K, respectively, indicating a transition to superparamagnetic behavior. The comparison of blocking temperatures for zinc ferrites, however, is ambiguous because of the difference in iron content and in the inversion degree of cation distribution. For the $ZnFe_2O_4$ sample, the blocking temperature is much lower than that measured for the other compositions, which indicates a wider temperature range of superparamagnetism for the $ZnFe_2O_4$ nanoparticles.

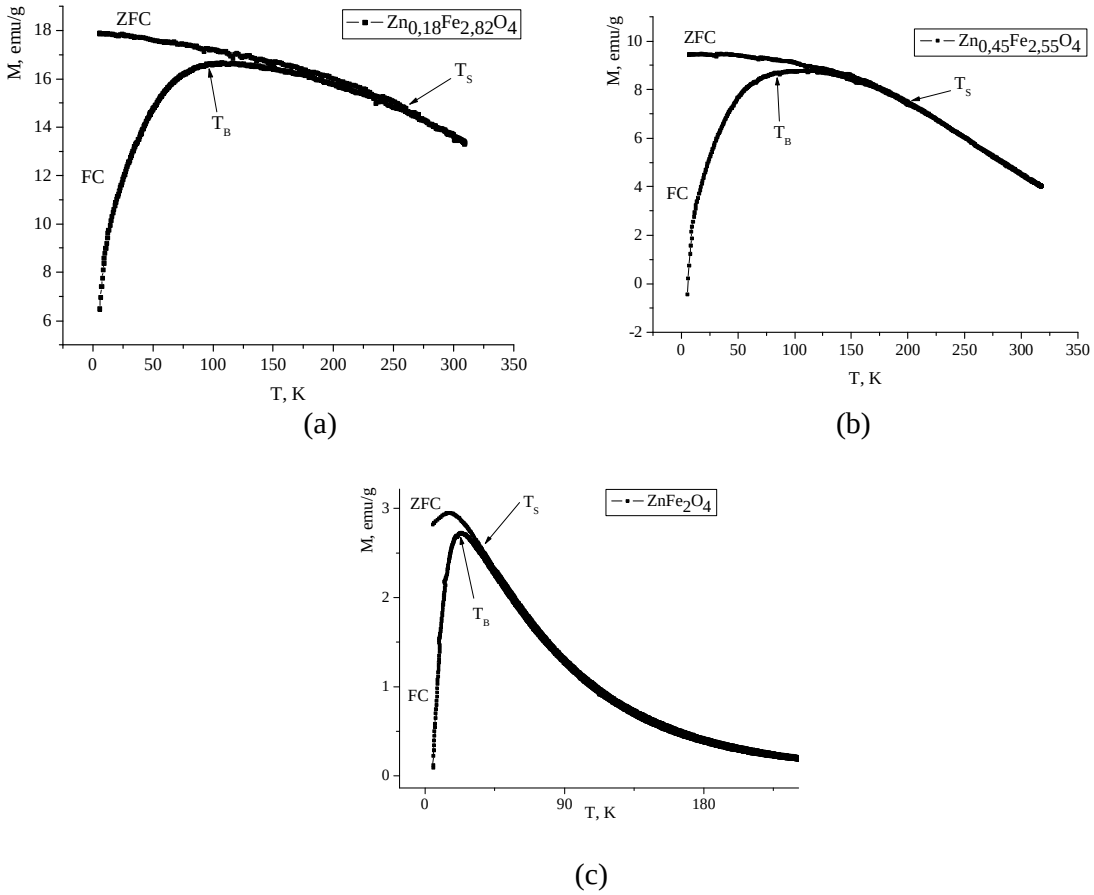

Fig. 6. ZFC and FC curves of $Zn_{0.18}Fe_{2.82}O_4$ (a), $Zn_{0.45}Fe_{2.55}O_4$ (b) and $ZnFe_2O_4$ (c); H = 60 Oe

4. Conclusion

Zinc-iron oxide nanoparticles ($Zn_xFe_{3-x}O_4$, x = 0, 0.18, 0.45, 1) were synthesized via modified inorganic sol-gel technique. The particles exhibit a crystallite size of 5-10 nm and superparamagnetic behavior at room temperature. IR spectroscopy data revealed the substitution of Fe^{3+} ions in tetrahedral sites of Fe_3O_4 spinel lattice with Zn^{2+} ions with the formation of single-phase solid solutions in a wide range of concentrations. Hysteresis behavior is observed for all samples at 5 K. The highest maximum magnetization of 59 emu/g at 300 K corresponds to $Zn_{0.18}Fe_{2.82}O_4$ sample, and at 5 K – to $Zn_{0.45}Fe_{2.55}O_4$ (86 emu/g), both exceeding the maximum magnetization of pure magnetite due to the dominant A□B cation interactions. This demonstrates that the chosen technique is applicable to the synthesis of zinc-iron oxide superparamagnetic nanoparticles with tunable magnetic properties.

References

1. Tartaj P., Puerto Morales M., Veintemillas-Verdaguer S., Gonzalez-Carreno T. and Serna C. J. // *J. Phys. D: Appl. Phys.* 36 (2003) R182-R197.
2. Mornet S., Vasseur S., Grasset F., Duguet E. // *J. Mater. Chem*. 14 (2004) 2161-2175.
3. Thorek D. L., Chen A. K., Czupryna J. and Tsourkas A. // *Ann. Biomed.Eng*. 34 (2006) 23-38.
4. Wan J., Cai W., Meng X. and Liu E. // *Chem. Commun*. 2007, 5004-5006.
5. Jordan A., Scholz R., Maier-Hauff K., Johannsen M., Wust P., Nadobny J., Schirra H., Schmidt H., Deger S., Loening S.A., Lanksch W. and Felix R. // *J. Magn. Magn. Mater*. 225 (2001) 118-126.
6. Hamdeh H. H., Ho J. C., Oliver S. A., Willey R. J., Oliveri G. and Busca G. // *J. Appl. Phys.* 81 (1997) 1851-1857.
7. Hochepied, J., Bonville, P., Pileni, M. // *J. Phys. Chem. B* 104 (2000) 905-912.
8. Wan J., Jiang X., Li H. and Chen K. // *J. Mater. Chem*. 22 (2012) 13500-13505.
9. Goldhaber S. B. // *Regul. Toxicol. Pharmacol.* 38 (2003) 232-242.
10. Chinnasamy C. N., Narayanasamy A., Ponpandian N., Chattopadhyaya K., Guerault H. and Greneche J.-H. // *J. Phys.: Condens. Matter* 12 (2000) 7795-7805.
11. Kamiyama T., Haneda K., Sato T., Ikeda S. and Asano H. // *Solid State Commun*. 81 (1992) 563-566.
12. Tanaka K., Makita M., Shimizugawa Y., Hirao K. and Soga N. // *J. Phys. Chem. Solids* 59 (1998) 1611-1618.
13. Yamamoto Y., Tanaka H. and Kawai T. // *Jpn. J. Appl. Phys.* Part 2, 40 (2001) L545-L547.
14. Azam A., Chaman M., Naqvi A.H. // *Int. J. Nanoparticles* 2 (2009) 388-393.
15. Nakashima S., Fujita K., Tanaka K. and Hirao K. // *J. Phys.: Condens. Matter* 17 (2005) 137-149.
16. Surinwong S., Rujiwatra A. // *Particuology* 11 (2013) 588-593.
17. Interrante L.V., Caspar L.A., Ellis A.B. *Materials chemistry. An emerging discipline*. – Washington: American Chemical Society, 1995. – 555 p.
18. Ivanovskaya M., Bogdanov P., Gurlo A. // *Proc. VIII Int. Meet. Chem. Sensors*, p. 94, Basel, Switzerland, 2000.
19. Brinker C.J., Scherer G.W. *Sol-gel science*, 502 p., AP, London, 1990.
20. Pankov V.V. // *Mater. Sci. Engineering* V. A224 (1997) 101-106.
21. Kotsikau D., Ivanovskaya M., Taurino A., Siciliano P. // Mater. Int. Conf. Nanomeeting-2007, Minsk, Belarus, 22-25 May / Ed. by V.E. Borisenko et al. – Singapore: World Scientific. – 2007. P. 372-376.
22. Gillot B., Benloucif R.M., Rousset A. // *J. Solid State Chem.* V. 39. № 4. (1981) P. 329-336.
23. Gillot B., Jemmali F., Rousset A. // *J. Solid State Chem.* V. 50. № 2 (1983) P. 138-145.
24. Mürbe J., Rechtenbach A., Töpfer J. // *Mater. Chem. Phys.* V. 110 (2008) P. 426-433.
25. Coey J.M.D., Khalafalla D. // *Phys. Status Solidi (a)* V. 11 (1972) P. 229-241.
26. Murbe J., Rechtenbach A., Topfer J. // *Mater. Chem. Phys.* V. 110 (2008) 426–433.
27. Sepalak V., Bergmann I., Feldhoff A., Heitjans P., Krumeich F., Menzel D., Litterst F.J., Campbell S.J., Becker K.D. // *J. Phys. Chem. C* V. 111 (2007) 5026–5033.